Turbulent transport of fast ions in the Large Plasma Device

Shu Zhou,[1] W. W. Heidbrink,[1] H. Boehmer,[1] R. McWilliams,[1] T. Carter,[2] S. Vincena,[2]
S. K. P. Tripathi,[2] P. Popovich,[2] B. Friedman,[2] and F. Jenko[3]
[1]*Department of Physics and Astronomy, University of California, Irvine, California 92697, USA*
[2]*Department of Physics and Astronomy, University of California, Los Angeles, California 90095, USA*
[3]*Max-Planck-Institut für Plasmaphysik, EURATOM Association, 85748 Garching, Germany*

Strong drift wave turbulence is observed in the Large Plasma Device [H. Gekelman *et al.*, Rev. Sci.
Instrum. **62**, 2875 (1991)] on density gradients produced by a plate limiter. Energetic lithium ions
orbit through the turbulent region. Scans with a collimated ion analyzer and with Langmuir probes
give detailed profiles of the fast ion spatial distribution and the fluctuating fields. The fast ion
transport decreases rapidly with increasing fast ion gyroradius. Unlike the diffusive transport caused
by Coulomb collisions, in this case the turbulent transport is nondiffusive. Analysis and simulation
suggest that such nondiffusive transport is due to the interaction of the fast ions with stationary
two-dimensional electrostatic turbulence. © *2010 American Institute of Physics.*
[doi:10.1063/1.3486532]

I. INTRODUCTION

The influence of microturbulence on fast ion behavior in plasmas has attracted growing interest in fusion and space physics. Fast ions are ions with energies that are much larger than typical thermal plasma ions. Confinement of fast ions is a critical issue in fusion experiments approaching ignition,[1] and many space and astrophysical problems (see, e.g., Ref. 2 and references therein) depend on understanding fast ion dynamics in a turbulent medium. Many fast ion transport measurements in tokamaks are consistent with classical theory, yielding lower-level diffusion compared to thermal ions.[3] But some recent tokamak studies[4,5] observe anomalous transport of fast ions, in seeming contradiction with earlier experimental results and theories.

A widely accepted explanation for the low transport of fast ions is that energetic ions phase average over the microturbulence structure along its large gyro and drift orbits.[6–8] Simulation publications describe transport of energetic ions with large Larmor radii in two-dimensional (2D) or three-dimensional turbulence, in cylindrical and toroidal geometry.[9–13] These investigations disagree on the mechanisms and scaling dependencies of transport: Some claim the orbit averaging is rarely operative,[10,11] while others suggest orbit averaging is generally valid for energetic ions.[12] Consequently the prediction of the scaling of fast ion diffusivity is not well explained.

Experimentally, the study of fast ion transport by microturbulence is challenging. Diagnostic tools in fusion devices usually are limited to noncontact, line, or volume averaged methods. In neutral-beam current drive experiments in ASDEX-Upgrade,[14] anomalous transport is inferred from the time evolution of the current profile.[4] In DIII-D,[15] spectroscopic and current-profile measurements provide evidence of transport in excess of neoclassical levels under some conditions.[16,17] Measurement in a toroidal magnetized plasma device (TORPEX) has begun.[18,19] In this paper, we report direct measurements of fast ion transport in the presence of drift wave turbulence. The Large Plasma Device[20] (LAPD) at UCLA provides a probe-accessible plasma with comparable dimension to magnetic fusion devices. In order to destabilize low-frequency drift waves, a density gradient was created by placing an obstacle in the chamber to block primary electrons from the cathode-anode source.[21] The approach discussed in this paper was to launch test-particle fast ion beams with narrow initial width in phase space and to have the fast ion gyro-orbit overlap with the turbulent potential structure of the drift wave. Then the fast ion beam was detected at different distances away from the fast ion source by a collimated ion analyzer. This allows study of fast ion transport in phase space with time and space resolution. This technique has been used in previous studies of fast ion classical diffusion[22] and of resonance with shear Alfvén waves (SAW).[23,24] In both studies, agreement with theoretical predictions is observed. In the present experiment, the energy and time dependencies of the fast ion transport in drift wave turbulence are studied on a relatively short time scale compared to the turbulence correlation time τ_c. Simulations using the resistive fluid-code BOUT (Ref. 25) and a Monte-Carlo test particle following code explain the experimental data.

The organization of this paper is as follows. The experimental setup and diagnostics of fast ions and drift wave turbulence are introduced in Sec. II. Major experimental results including measurement of fast ion transport as a function of time and energy are reported in Sec. III. In Sec. IV, analytical models are presented to explain the experimental data. Simulation results appear in Sec. V. Conclusions are drawn in Sec. VI.

II. EXPERIMENTAL SETUP

A. Overview

The experiment is performed in the LAPD (Ref. 20) at UCLA. The plasma column in LAPD is generated by dc discharge pulses between a barium oxide coated cathode and a molybdenum mesh anode. The discharge time is ~10 ms,
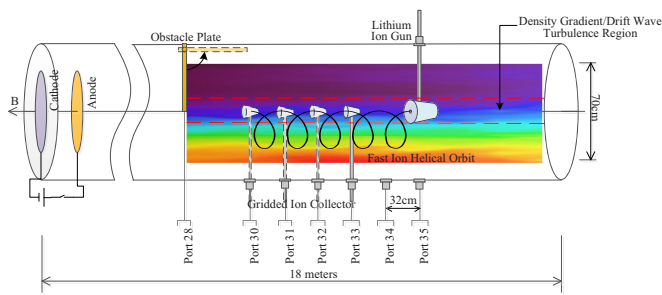
FIG. 1. (Color online) Experimental setup in the LAPD. Fast ions interact with drift wave turbulence in the region between the two dash lines. The probe is inserted at different ports each time to study the spatial dependence of transport. The ion source and analyzer are axially aligned. The contour shows a typical density profile when plate-obstacle is deployed.

with 1 Hz repetition rate. The plasma column has a diameter of 70 cm and is 17 m long. The axial magnetic field is uniform with $B_z \sim 1.2$ kG Typical parameters of the LAPD plasma during discharge are $n_e \sim 2.0 \times 10^{12}$ cm^{-3}, $T_e \sim 5$ eV, and $T_i \sim 1$ eV. The line-integrated plasma density is measured by an interferometer. A triple Langmuir probe[26] is used to measure the spatial profile of the plasma density, temperature, floating potential, and their fluctuations. The experimental setup and the typical fast ion trajectory are shown schematically in Fig. 1. A rotatable, floating copper plate-obstacle blocks half of the plasma column. (The plate can rotate out of the column to create a quiet reference condition.) A steep density gradient, along with large density fluctuations ($\delta n/n \sim 1$), is observed at the edge region in the shadow of the plate. Figure 2 shows the spatial profile of the density (n_e) and density fluctuation level (characterized by the standard deviation of the density) behind the plate during the ~ 10 ms discharge time, where the plate edge is at $x = 0$. The density gradient has a transverse scale length of ~ 5 cm (the background ion sound radius $\rho_s \sim 0.6$ cm and the ion gyroradius $\rho_i \sim 0.24$ cm). No ionizing fast electrons from the cathode-anode discharge are present in the area be-

hind the plate, so that no volume ionization occurs. Therefore, the observed plasma density behind the plate is due to cross-field transport.
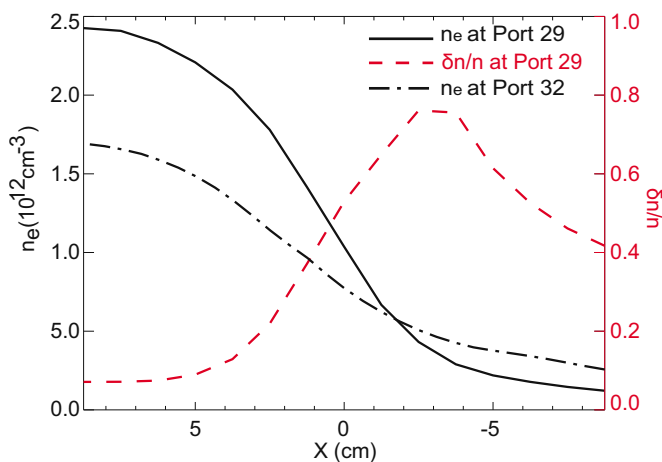
The lithium ion source[27] and detector used in this experiment have been tested and successfully used in the previous investigation of fast ion cyclotron resonance with SAW.[23] The lithium ion source is inserted into the LAPD plasma via a rectangular side port (port 35). Both the shaft and housing of the source are floating to minimize the perturbation to the main plasma column. With a 5 mm exit aperture, the ion source launches a low divergence ($\sim \pm 5°$) Li-7 ion beam. The beam energy is controlled by the bias voltage on the emitter, ranging from 400 eV up to 1 keV with a fluctuation level of ± 5 eV. Typical beam current densities are ~ 300 μA/cm^2. Intermediate grids between the emitter and the exit aperture provide an acceleration-deceleration[27] configuration to assure sufficient current at low beam energy.

The fast ion source is operated at various pitch angles with respect to the magnetic field. Thus the trajectories of fast ions are helical: gyromotion perpendicular to the magnetic field and parallel motion with constant velocity v_z along the magnetic field. The fast ion parameters are carefully chosen to make

$$d_{port}/v_z = T_f, \tag{1}$$

where $d_{port} = 31.95$ cm is the distance between each two diagnostic ports and T_f is the fast ion gyroperiod. This way, the initially slightly divergent beam is refocused at each observation point.

A collimating fast ion analyzer[28] is inserted at four different locations (2–5 ports away from the source) to measure the spreading of the ion beam as a function of distance. The fast ion analyzer is composed of a 3 mm copper disk collector, an identical dummy collector (to minimize common mode noise), and two molybdenum retarding grids. It is designed to reject thermal particles electrically and geometrically. Operated at the same pitch angle as the ion source, the analyzer is collimated to the direction of the fast ion beam to maximize the beam signal. The angular acceptance of the analyzer is limited to $\pm 15°$ by its geometry. Mounted on a computer-controlled 2D probe drive system, the ion analyzer is able to scan within a perpendicular plane to precisely contour the beam profile with ± 0.5 mm accuracy. The fast ion current and dummy pickup signal are fed into a differential amplifier with 1 MΩ input impedance. The bandwidth of the collected signal is limited to ~ 5 kHz by the resistance-capacitance (RC) time of the transmission circuit. Synchronization of the fast ion source, the LAPD discharge pulse, and the data collection system is critical for studying wave-particle interaction. To create large amplitude drift wave turbulence, the experiment was performed during the active discharge, which is the first ~ 10 ms of each LAPD cycle. The active discharge, compared to the afterglow, has a larger plasma density ($\sim 2.5 \times 10^{12}$ cm^{-3}) and higher plasma temperature ($T_e \sim 5$ eV, $T_i \sim 1$ eV), thus is suitable for creating a large density gradient. Figure 3(a) shows an example of the plasma density variation during the data collection time. It should be noted that during the active discharge, the collected signal-to-noise level is much lower compared to the

FIG. 2. (Color online) Horizontal profiles of density at two different axial positions (solid and dash-dot lines) and of density fluctuations (dashed line), averaged between 2–6.5 ms in the active discharge. The edge of the plate-obstacle is at $x=0$, and the ionizing fast electrons are blocked in the $x>0$ region.
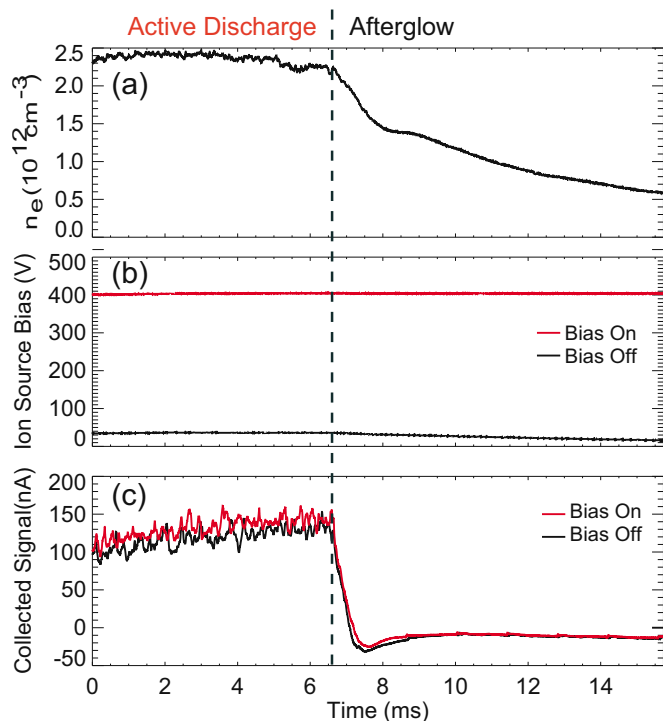
FIG. 3. (Color online) Typical time evolution of (a) plasma density, (b) ion source operating voltage, and (c) collected signal during the data collection time window. The active discharge ends at ~6.5 ms. (a) Line-averaged plasma density measured by the interferometer. (b) Operating voltage on the ion source to launch a 400 eV ion beam. (c) Collected signal when the ion source operating voltage is on/off. The fast ion signal is the difference between these two. Signal collected three ports from the source.

afterglow, due to the large background density fluctuation. To facilitate the extraction of the small beam signal from the large background plasma noise, the fast ion source is operated at half the LAPD discharge frequency by turning the ion source emitter bias on and off, and the difference between the signals is recorded. A sample emitter bias and the corresponding analyzer signal are shown in Figs. 3(b) and 3(c). The difference signal between bias on and off discharges yields the actual fast ion current. To further increase the signal-to-noise ratio, the signal is averaged over an even number of shots (usually ten shots) at the same spatial location.

B. Drift wave characteristics

Drift waves associated with a steep density gradient have been studied extensively in the LAPD.[21,29] Drift wave characteristics are diagnosed using radial inserted Langmuir probes and B-dot probes.[30] Two triple Langmuir probes, separated axially by 95.85 cm, are used to analyze the parallel and perpendicular (to the magnetic field) correlation of the drift wave turbulence. The contour plot in Fig. 4(a) shows the transverse spatial distribution of the density turbulence amplitude. The corresponding spatial averaged fast Fourier transform power spectrum of the fluctuations is shown in Fig. 4(b). The phase velocity of the drift wave,[31] can be estimated as
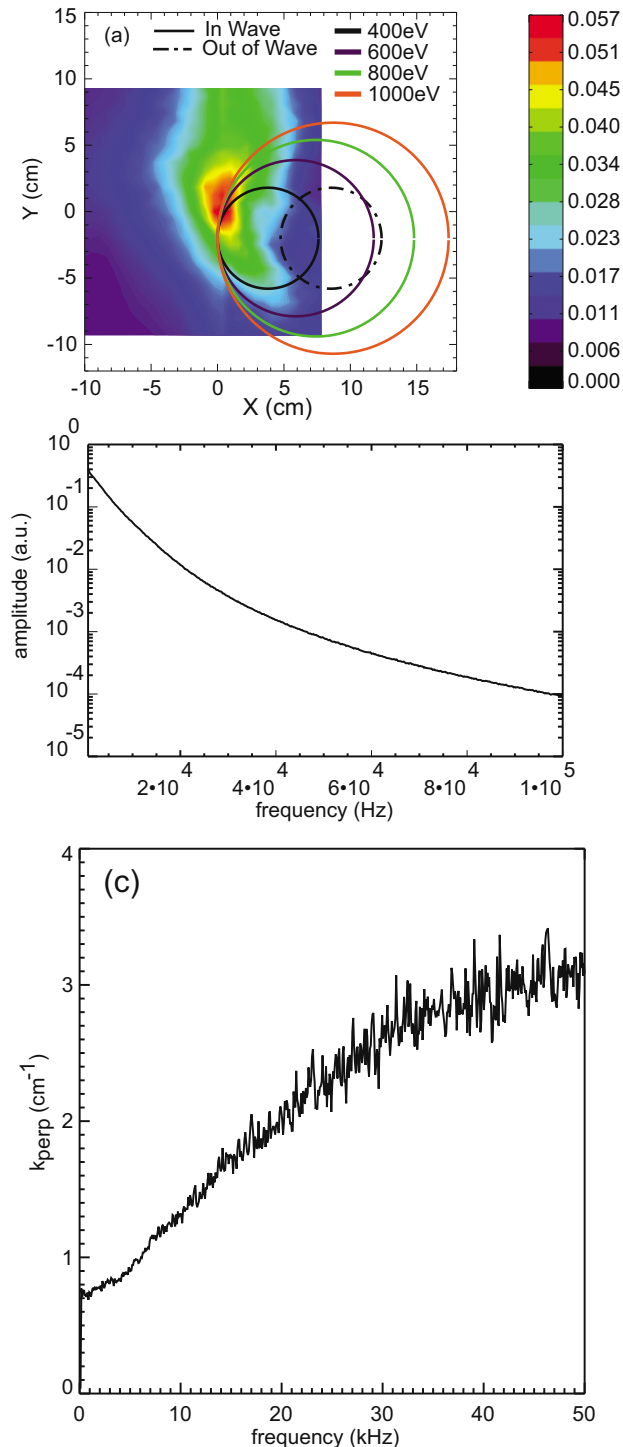
FIG. 4. (Color online) Characteristics of drift wave turbulence created by the plate-obstacle. (a) Contour of the total power of the wave with frequency ranges of 0.7–100 kHz, fast ion orbits with different energies is overlaid to show the overlap between the waves and particles. (b) Averaged fluctuation power spectrum (log-log). (c) Dispersion relation of the wave, calculated from the cross-correlation between two triple probes.

$$v_{De} = \frac{KT_e}{eB_0} \frac{n_0'}{n_0} \sim 1 \times 10^3 \ \mathrm{m/s},$$

agrees with the slope of the measured wave dispersion relation [Fig. 4(c)]. Within the accuracy of axial alignment of the two triple probes separated by 95.85 cm, small phase differ-
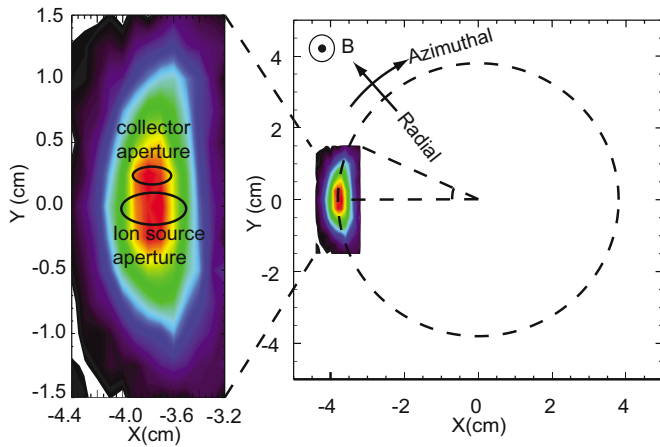
FIG. 5. (Color online) (right) Projection of the fast ion orbit onto the horizontal plane, with the beam profile measured three ports from the source overlaid. (left) Detail of the beam profile, together with the projection of the ion source and collector apertures.

FIG. 6. (Color online) A typical collected beam profile and data analysis process. (a) Contour of the signal amplitude. Dotted line: fitted gyro-orbit. Solid line: mesh imposed to calculate the beam FWHM. (b) Beam radial profile and its gauss fit. (c) Beam azimuthal profile and its gauss fit.

ence ($\sim 8°$) is observed between the two signals, thus $k_\parallel \cong 0$ can be assumed. *B*-dot probe measurements show a much lower level of magnetic fluctuation ($\delta B \sim 0.1$ G), indicating that the wave is mainly electrostatic.

Spatial alignment between the drift wave turbulence and the fast ion orbit is crucial to optimize wave-particle interaction. The lithium ion source, the ion analyzer, and the region of large turbulence amplitude are axially aligned. The fast ion orbits for different energies, projected onto Fig. 4(a), are carefully adjusted to make the best overlap with the turbulent wave, denoted as "in wave" (solid line). For the in wave case, the fast ion beam is affected by both the turbulent wave and Coulomb collisions. In order to separate the effect of the wave turbulence on beam spreading, the fast ion source is shifted horizontally by 5 cm to remove the orbit from the strong turbulence region; this reference case is denoted as "out of wave" (dashed line). The Coulomb collision effect on beam spreading is comparable for both cases. Thus the difference in beam spreading is exclusively caused by the transport induced by wave turbulence. The classical Coulomb collision effect is also confirmed by recording the beam spreading with the plate-obstacle turned out of plasma.

C. Beam profile analysis

A typical beam profile is shown in Fig. 5 where the collected beam spot size is compared to the transverse orbit size. The aperture size of the ion gun is 0.5 cm. The analyzer has an aperture of 0.3 cm.

To obtain an accurate quantitative measurement of fast ion diffusion, the 2D beam signal array from the collector is analyzed to yield the radial and azimuthal profile separately. Figure 6 demonstrates a typical analysis of the beam profile. First, the beam trajectory is fitted into the observed contour plot with its gyroradius [dashed line in Fig. 6(a)], using Gaussian centers of all the row profiles along the *x* direction (blue diamonds). Then a fine grid along the fitting orbit is developed (solid lines) and the beam profile is projected to the grid. The weight of each radial and azimuthal profile along the new grid is calculated by the χ^2 goodness of its
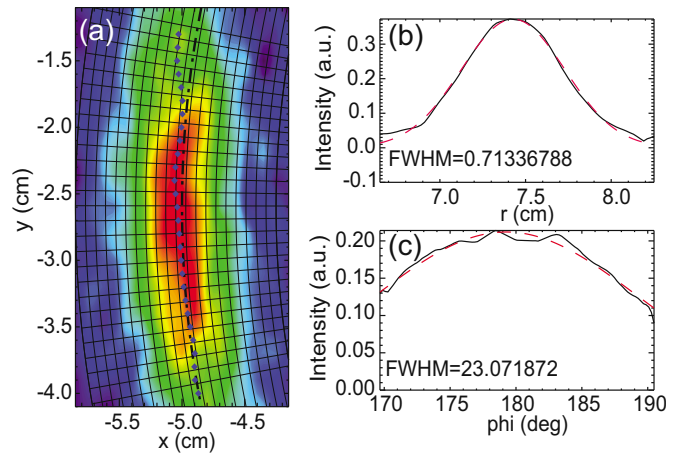
Gaussian fits. By averaging over all radial and azimuthal profiles, the weighted average radial profile and azimuthal profile are obtained. Finally, a Gaussian fit is performed on the averaged profile to obtain its full width at half maximum (FWHM) [Figs. 6(b) and 6(c)].

The finite angular acceptance of the collector ($\pm 15°$) affects the profiles in the azimuthal direction but not in the radial direction. For one experimental condition shown below, the profile was remeasured with an analyzer that accepts incident ions from a broader range of angles. With this analyzer, the azimuthal profile is longer but the radial profile is unaffected, confirming that the radial profiles accurately represent the actual beam width.

III. EXPERIMENTAL RESULTS

A. Energy dependence of radial transport

Lithium 7 ion beams with four different energies (400, 600, 800, and 1000 eV) are launched and collected three ports (95.85 cm) away to study the energy dependence of fast ion transport. By changing the pitch angle, ions with different energies are forced to have the same parallel velocity v_z, which is determined by Eq. (1); only the perpendicular energy changes. Detailed parameters for these four cases are listed in Table I. Typical time scales listed in Table II shows that, in this experiment, the fast ion cyclotron period is much shorter than the typical drift wave period or the correlation time of the turbulence.

TABLE I. Parameters of the fast ion orbits for the four conditions studied in the experiment.

Energy (eV)	$E_\parallel$ (eV)	E_{perp} (eV)	Pitch angle θ (deg.)	R_{gyro} (cm)
415	258	157	36.76	3.8
570	258	312	49.14	5.9
800	258	542	55.49	7.4
1000	258	742	59.55	8.7

TABLE II. Comparison of different time scales.

Transport related time scales	Time (ms)
Cyclotron period $\tau_{cyclotron}$	3.8×10^{-3}
Pitch angle scattering time τ_{pas}	5
Turbulence correlation time $\tau_{correlation}$	~ 10
Drift wave period	0.1–10
Averaging time of the data	10

Figure 7 shows the 2D contour plots of the beam profiles collected three ports away from the ion source when the plate-obstacle is positioned to block half of the plasma column and the fast ion orbit overlaps the turbulence wave region. Its FWHM is shown as the in wave case (diamonds) in Fig. 8. In Fig. 7, the contour of the beam spatial profile has a clear dependence on the fast ion energy. Greater fast ion transport is observed at lower beam energy. Note that the vertical length of the beam spot is limited by the angular acceptance of the fast ion analyzer and does not describe the real beam azimuthal diffusion. Thus only the radial spreading of the beam is investigated. The radial FWHMs of the beam with and without the influence of drift waves show significant differences, especially at low beam energies (Fig. 8). The energy dependence of the beam FWHM is consistent with the observed original beam contour in Fig. 7.
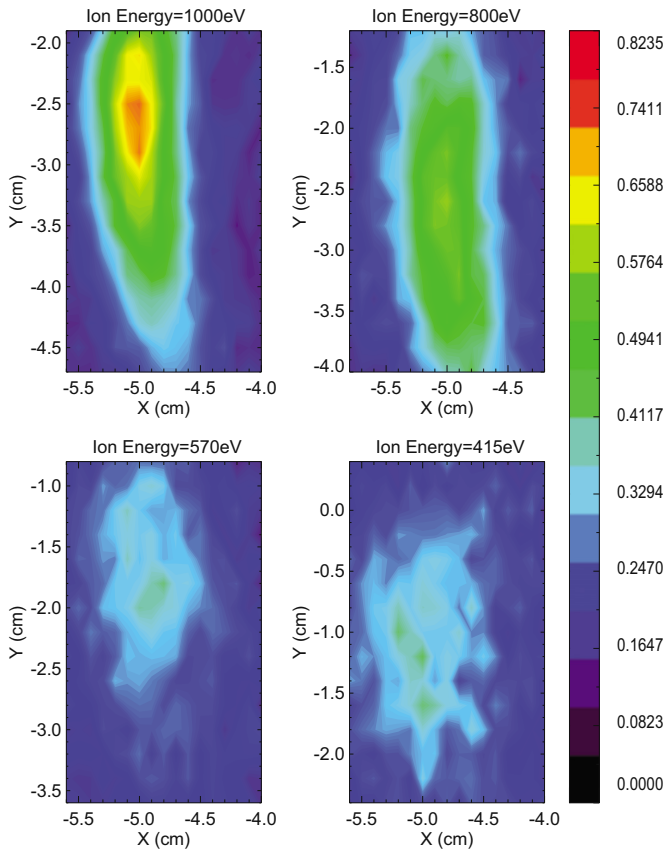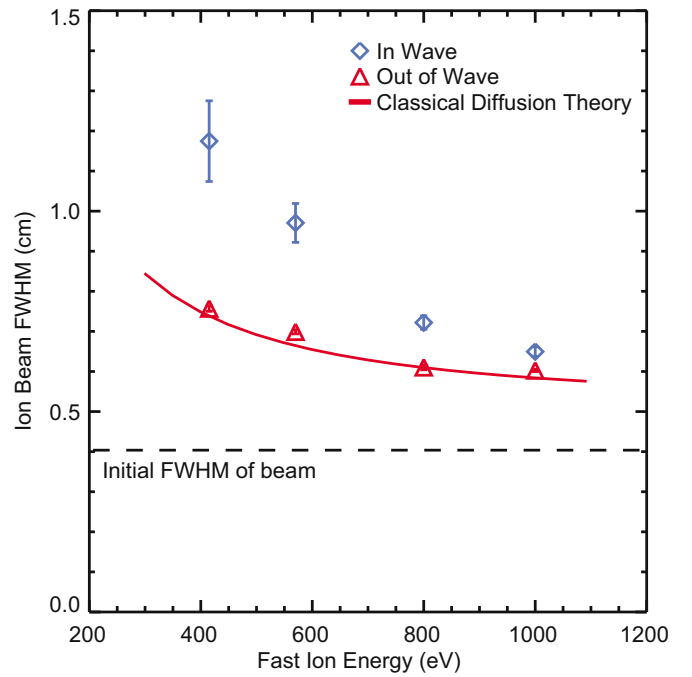
FIG. 8. (Color online) Beam FWHM vs energy with the plate inserted (diamond) and retracted (triangle). The solid line shows the dependence predicted by classical diffusion theory. The dashed line is the initial beam width caused by the finite aperture size of the ion source.

The error bars shown in Fig. 8 are statistical error calculated among data taken at ten consecutive LAPD discharges. During each discharge, 4000 samples, taken in ~ 10 ms, are averaged to get the beam signal at a certain spatial location. The signal is also averaged by the RC time constant of the transmission circuit. The averaging of the signals filters out high frequency information but greatly increases the signal-to-noise ratio. Systematic errors include the axial and pitch alignment between the ion source and the ion analyzer. The axial alignment is carefully done with a telescope at the end viewpoint of LAPD. The pitch angles are adjusted by a digital level with $\pm 0.1°$ accuracy. Other possible errors include the fluctuation of the initial beam energy (± 5 eV) and angular divergence ($\sim 3°$).

Besides the turbulence induced transport, the fast ion beam is always Coulomb scattered by the background plasma, resulting in classical diffusion of the beam. In this experiment, the beam spatial profiles are also recorded for reference when the plate-obstacle is retracted, shown as out of wave data in Fig. 8.

The classical diffusion of fast ions in the LAPD plasma has been extensively studied, and expressions of the diffusivity have been developed theoretically and verified experimentally.[22] According to classical theory, the cross-field transport of particles is due to the pitch angle scattering with the background plasma in phase space, and the diffusivity is proportional to the background density. A theoretical prediction (solid line in Fig. 8) of the classical diffusion effect [following Eq. 12 in Ref. 22] is found to agree quantitatively with the out of wave data. Consequently, induced beam transport due to the background plasma turbulence, which is always present in the nonequilibrium LAPD plasma

FIG. 7. (Color online) Typical beam profiles for different fast ion energies, collected three ports (95.85 cm) away from the ion source.
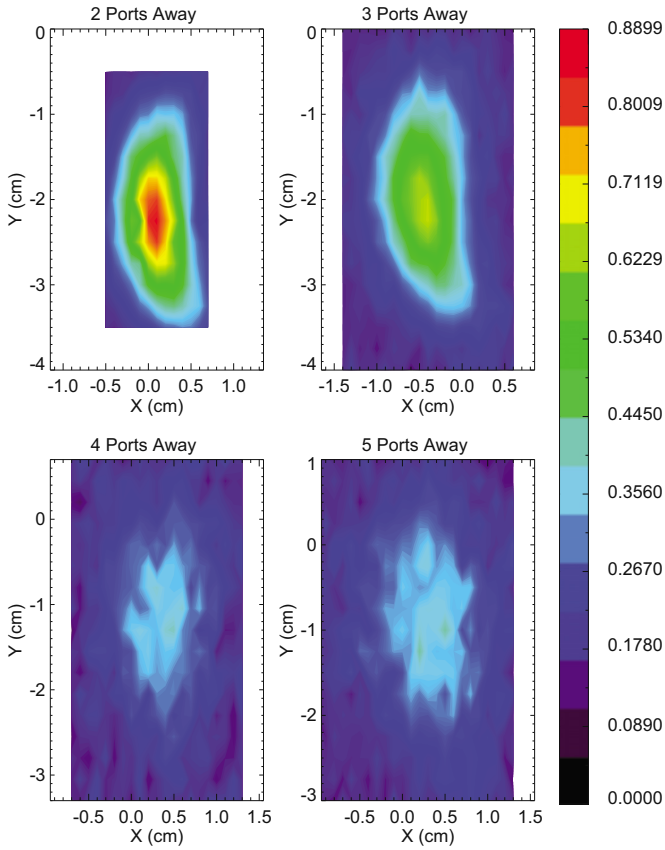
FIG. 9. (Color online) Beam profile collected at different distances away (2–5 ports/31.95–159.75 cm) from the ion source.

FIG. 10. (Color online) The square of the radial ion beam FWHM vs distance from the source. The out of wave data are fitted by a linear function. The in wave data are fitted by a polynomial function of second order.

during the active discharge, can be neglected for the out of wave case. In the in wave case, the fast ion beam is affected both by Coulomb collision and drift wave turbulence. Note that, the averaged background plasma density along the fast ion trajectory is lower by ∼50% for this case due to density depression by the plate-obstacle, and the classical diffusivity is expected to be reduced by ∼50%. The fast ion transport in this case is mainly due to interaction with drift wave turbulence.

B. Time dependence of radial transport

The fast ion beam signals are collected at 2–5 ports (63.9–159.75 cm) away from the ion source to study the time dependence of the beam radial transport, which, in this case, is equivalent to the spatial dependence. Because the fast ion parallel velocity is nearly constant for all energies, its total traveling time is proportional to the number of ports it passes. Contour plots of 400 eV beam profiles at different distances from the ion source are shown in Fig. 9. Radial transport of the beam versus distance is observed, while the azimuthal spreading is not shown due to the limitation of the ion analyzer. The radial FWHM of the contours are displayed in Fig. 10. The square of the FWHM is plotted in the figure to make a better comparison possible with the analytical models.

For the out of wave case, the fast ion beam spreading is due to Coulomb scattering, as discussed in Sec.III A In this case, with uniform axial speed, the time of travel t for an ion

may be described by the axial distance traveled. In other words, by noting the number of axial ports, N, separating the ion beam source from the analyzer, the time t may be estimated if the parallel beam speed is known. Hence, a diffusive process would have $(\Delta r)^2 \propto t \propto N$. The proportionality constant between the diffusion coefficient and t was worked out[32] and experimentally confirmed in LAPD.[22] The data points are fitted to optimal curves to demonstrate their functional dependence on the traversed distance. Following Eq. 7 in Ref. 22, a linear fit

$$\text{FWHM}^2 = 8 \ln 2(\langle \Delta r_0^2 \rangle + 2D_\perp t) \qquad (2)$$

for the out of wave data shows a diffusive nature of Coulomb scattering induced transport, with diffusivity $D_\perp = 2460 \ \text{cm}^2/\text{s}$.

In the in wave case, the density along the fast ion orbit is depressed by the plate-obstacle. Considering $D_\perp \propto n_{i,e}$, the estimated diffusivity due to Coulomb scattering is

$$D_\perp{}' = 1210 \ \text{cm}^2/\text{s}.$$

For this case, a discrepancy between the beam FWHM (diamonds) and the classical diffusion theory (dash dot line) is observed. The beam transport is much larger than predicted by classical theory, indicating that turbulent transport dominates. Moreover, the in wave data cannot be fitted by a linear function. As discussed below, this reflects the nondiffusive nature of the transport.

IV. DISCUSSIONS OF THE EXPERIMENTAL RESULTS

Since the turbulence wave frequencies we studied satisfy $\omega \ll \Omega_{ci}$, and the fast ions only execute a few gyro-orbits, the

turbulent electric fields are static on the fast ion time scale. Also, the typical parallel wavelengths of the drift waves are long compared to the parallel distance of the fast ion trajectory. Thus an approximate model for the current experiment is that, each fast ion trajectory is affected by a quasi-2D, temporally constant electrostatic turbulent field. Different fast ions encounter changing realizations of the wave field, which randomizes the transport and results in the radial expansion of the beam spot.

The fast ion transport in such electrostatic turbulence is induced by two effects: change of fast ion gyroradius due to change in particle perpendicular energy $v_\perp$, and drift of the fast ion gyrocenter due to the turbulent electric field. The change in perpendicular energy follows the potential difference $\partial_t\phi$ during a gyrotransit. One may estimate the change of the fast ion perpendicular energy $\Delta E_\perp \sim e\Delta\phi \sim (n_1/n_0)KT_e \sim KT_e$. Here we assume $n_1/n_0 \sim 1$ consist with the density fluctuation measurement. The observed plasma potential fluctuation behind the plate-obstacle is ~ 10 V, which confirms the above estimate. Then the particle transport in radial direction associated with the energy change is

$$\Delta r \sim \Delta\rho_f \sim \frac{1}{\Omega_f}\left(\sqrt{\frac{2(E_\perp + KT_e)}{m_f}} - \sqrt{\frac{2E_\perp}{m_f}}\right)$$

$$\sim \rho_f \cdot \frac{KT_e}{2E_\perp}.$$

For fast ion energy ~ 400 eV and electron thermal energy ~ 10 eV, $\Delta r \sim 0.046$ cm, which is much smaller than the observed transport induced by wave. On the other hand, the gyrocenter drift induced by the fluctuating potential during each transit can be estimated as

$$\Delta r_E \sim \frac{\delta E}{B}\frac{2\pi}{\Omega_{ci}} \sim 0.3 \text{ cm}$$

with δE as the fluctuating electric field. This is of the same order as the observed beam spreading. Thus the perpendicular energy of fast ion is approximately constant, and the transport is mainly induced by the drift of the fast ion gyrocenter.

A. Gyroaveraging

The energy dependence of the beam FWHM for in wave (diamonds in Fig. 8) can be explained in terms of the so-called gyroaveraging effect. Since the gyromotion is much faster than the turbulent wave frequency, and the drift of the gyrocenter during each cyclotron period is small compared to the gyroradius, the gyroaveraging approximation can be applied.[6] The turbulent potential ϕ is then substituted by an averaged $\bar\phi$ over the gyro-orbit

$$\bar\phi(x) = \sum_k \phi_k e^{ikx} \cdot J_0(k_\perp\rho), \qquad (3)$$

which results a reduction in the potential fluctuation. In our experiment, $k_\perp\rho$ is of the order of 1, thus neither larger or small argument expansion can be applied. To estimate the gyroaveraging effect, the cross-correlation of ion saturation currents between two triple probes [Fig. 11(b)] is used to
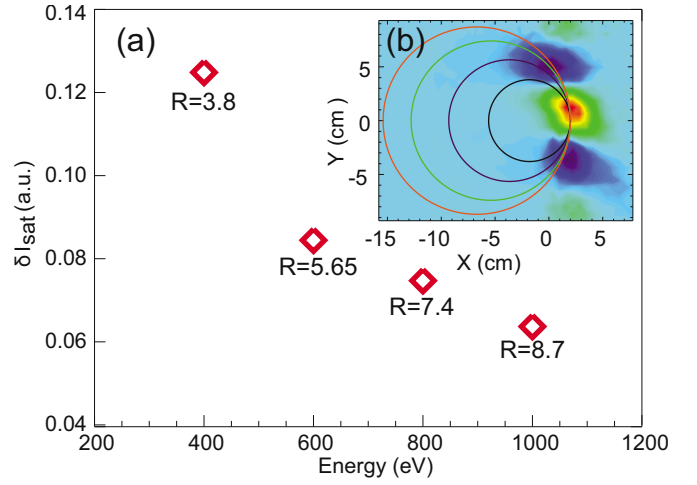
FIG. 11. (Color online) (a) The gyroaveraged density fluctuation shows a large reduction of fluctuation amplitude, and the fluctuation amplitude decreases with increased fast ion energy. (b) The cross-spectrum of the drift wave, measured by two triple probes two ports away (63.9 cm) from each other. The four measured gyroradii are overlaid.

indicate the turbulence mode structure and relative wave amplitude at different wavelength, and the gyroaveraging approximation is imposed to calculate the reduced potential due to averaging along different gyro-orbits. Here we assume that, for electrostatic drift waves, the fluctuation of the electric potential is proportional to the fluctuation of the plasma density, and that the density is proportional to the ion saturation current of the Langmuir probe measurement. Figure 11(a) shows the relative density fluctuation amplitude due to averaging over gyro-orbits of different energies (400–1000 eV), which are characterized by δI_{sat} along the gyrocenter positions. The gyroaveraged fluctuation is reduced at large beam energy, which agrees qualitatively with the energy dependence of the beam FWHM broadening.

B. Nondiffusive transport due to wave-particle correlation

The time dependence of the FWHM spreading (diamonds in Fig. 10) shows a nondiffusive nature of the radial transport. The data when the drift waves are on do not lie on a linear curve, indicating that the diffusivity D is not constant. The nondiffusive transport, also referred to as ballistic transport, of ions with large Larmor radii has been discussed in several theoretical papers,[9,13] and is related to the correlation between waves and fast ions. Generally, the diffusion coefficient of a transport procedure can be expressed as[33]

$$D(t) = \int_0^t d\tau \cdot L_{ii}(\tau), \qquad (4)$$

where $L_{ii}(t) = \langle v_i(0,0)v_i(x,t)\rangle$ is the Lagrangian autocorrelation function of the respective particle velocity. The transport is ballistic when $v_i(0,0) \cong v_i(x,t)$, by which L_{ii} is constant and $D(t) = \alpha t$.

L_{ii} in this experiment is closely related to the correlation between waves and fast ions. The fast ion velocity could be expressed as $v_i(x,t) = v_c + v_E(x,t)$, where v_c is the cyclotron

(a)

$$\bar{\upsilon}_E \cdot \tau_{cyclotron}$$

(b)
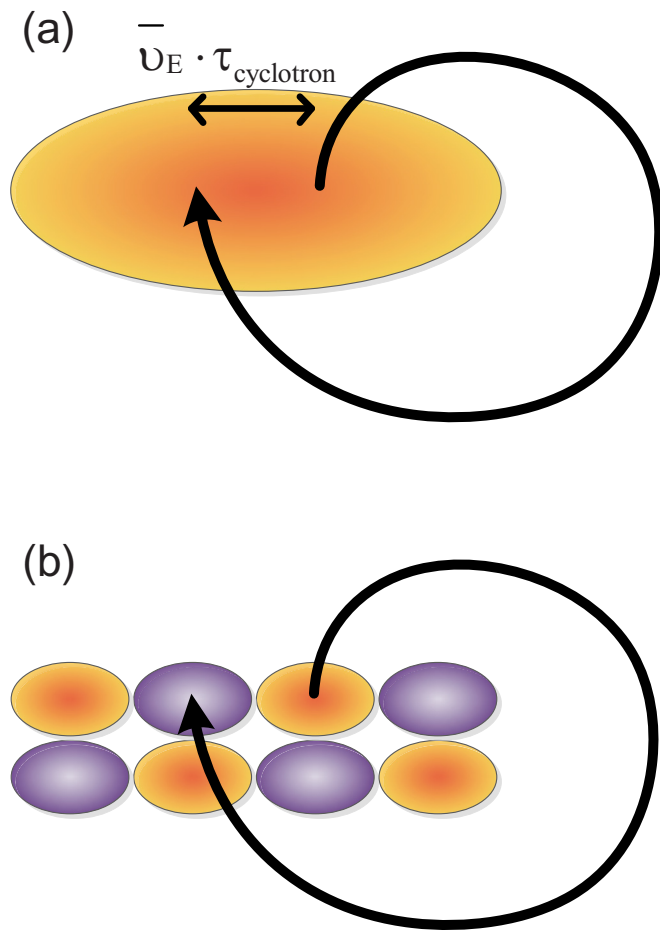
FIG. 12. (Color online) (a) The fast ion is correlated with the turbulent potential structure if the drift of gyrocenter during each cyclotron orbit is much smaller than the correlation length of the turbulence. (b) The fast ion is easily decorrelated with the wave if the drift is comparable with the correlation length of the turbulence, thus the fast ion orbit samples a different turbulent potential structure during each cyclotron orbit.

velocity associated with its perpendicular energy, which is approximately constant; $\upsilon_E(x,t)$ is the drift velocity of its gyrocenter associated with the turbulent E field it samples during the whole gyro-orbit. Thus $L_{ii} \cong \langle \upsilon_E(0,0)\upsilon_E(x,t)\rangle$. As the wave turbulence is static in the fast ion transition time scale, the spatial correlation between the fast ion orbit and the turbulent potential structure determines L_{ii}. As illustrated in Fig. 12, if $\bar{\upsilon}_E t < L_c$ [Fig. 12(a)], with L_c as the spatial correlation length of the turbulence, the fast ion orbit always samples approximately the same turbulent potential structure. Thus $L_{ii} \cong$ const, and the gyrocenter drift is ballistic. When $\bar{\upsilon}_E t > L_c$ [Fig. 12(b)], the orbit starts to sample a different potential structure, which randomizes υ_E and induces a diffusive transport. In the current experiment, the total broadening of the beam is ~ 1 cm within five gyro-orbits, $\bar{\upsilon}_E t_c \sim 0.2$ cm per orbit, and the typical $L_c \sim 5$ cm. Thus decorrelation between the fast ion trajectory and the turbulent potential does not happen, the averaged drift velocity $\bar{\upsilon}_E$ is approximately constant during the whole particle trajectory, and $L_{ii} \cong \bar{\upsilon}_E^2$. The diffusive coefficient for the turbulence induced transport is then
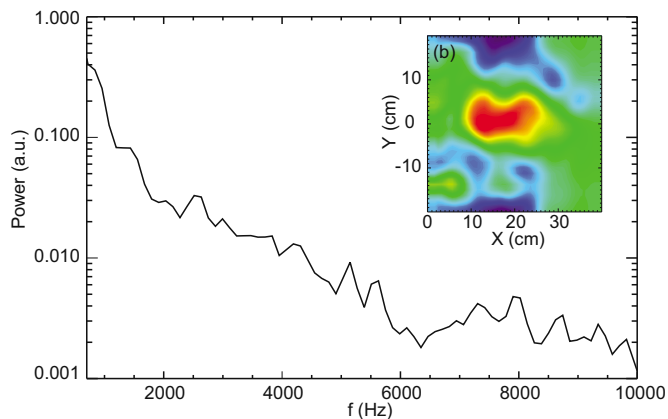
FIG. 13. (Color online) The characteristics of drift wave turbulence simulated by the BOUT code. (a) Fluctuation power spectrum. (b) Cross-correlation of the potential fluctuation.

$$D_{dr}(t) = \bar{\upsilon}_E^2 t. \tag{5}$$

The total beam FWHM, considering its initial width and classical diffusion,[22,32] is

$$W_{FWHM}^2 = 8 \ln 2[\langle(\Delta r_0)^2\rangle + 2(D_{cl} + D_{dr})t]$$

$$= 5.545[\langle(\Delta r_0)^2\rangle + 2D_{cl}t + 2\bar{\upsilon}_E^2 t^2]. \tag{6}$$

Using Eq. 12 in Ref. 22 as the classical diffusivity D_{cl}, this expression fits the in wave data very well (blue solid curve in Fig. 10), proving the validity of the above model and analysis. This analytic model is confirmed by the more detailed simulation of Sec. V.

V. SIMULATION RESULTS

A numerical simulation is performed to model the transport of fast ions in the turbulent drift wave field using a combination of the BOUT code and a test particle tracer code. BOUT was developed to model tokamak edge turbulence using collisional fluid equations, and was recently modified[34] to model the cylindrical LAPD plasma. The drift wave turbulence is simulated using fixed-profiles in BOUT by subtracting out the azimuthal average of the fluctuating density at each time step, preventing turbulent transport from relaxing the profile.[34] This technique in effect assumes that density fluctuations are small compared to the mean value and fails in the presence of strong fluctuations. Because of this, a shallower gradient than the actual experimental profile was used in the simulations. Simulations using particle sources and sinks which allow full nonlinear evolution of the profile are possible in BOUT and will be pursued in future work.[34] The other input parameters are the same as the experimental conditions in order to achieve a reasonable comparison with the experimental data. Figures 13(a) and 13(b) show the frequency spectrum and cross-field correlation function of the potential fluctuation calculated with the BOUT code. It is qualitatively consistent with the previously discussed experimental results [Fig. 4(b)]. As in the experiment, the spectrum predicted by BOUT is dominated by low-frequency turbulence (0.1–10 kHz) but the calculated spectrum is narrower than the observed one. The correlation length (~ 10 cm) agrees
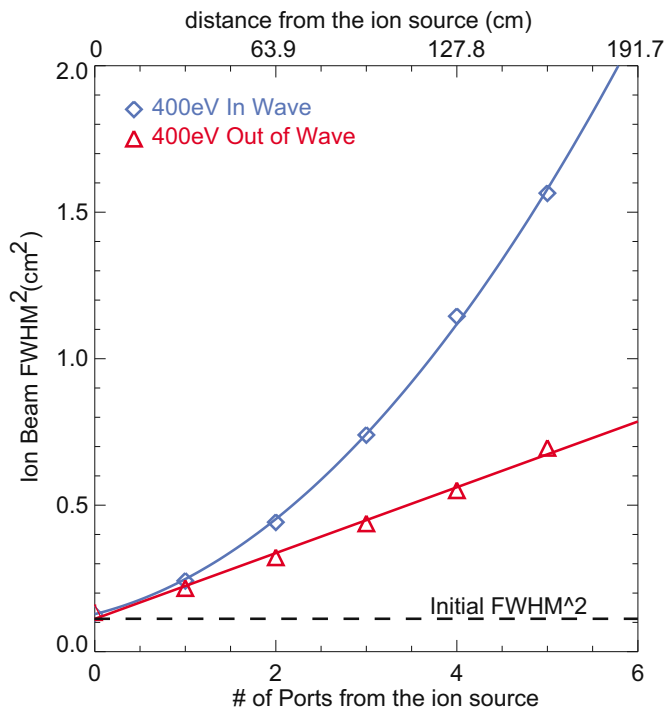
FIG. 14. (Color online) Monte-Carlo simulated fast ion FWHM (Ref. 2) as a function of distance (time). Triangles denote the effect of the classical transport, and is fitted by a linear function. Diamonds denote the effect of both turbulent wave and classical transport, and is fitted by a polynomial function of second order.

FIG. 15. (Color online) The trajectory of an individual guiding center in a representative turbulent potential structure. The triangles and diamonds show the fast ion GC position after each cyclotron orbit, 0–5 ports away from the ion source for turbulence with large triangle and small diamond amplitude.

well with the measurement from the triple probe [Fig. 11(b)]. The amplitude is smaller than in the experiment, presumably because the density gradient employed in the calculation is less steep. The wave electric field is derived from the potential profile and the amplitude of the field is multiplied by a factor to match the experimental measurement.

The spatial fluctuation spectrum of the BOUT result is then imported into a Monte-Carlo code to simulate the fast ion behavior in the calculated wave fields. The fast ion beam density in our experiment is typically $\sim 5.0 \times 10^8$ cm^{-3}, and is 3–4 orders of magnitude smaller than the background plasma density. Thus the fast ions can be treated as test particles in the code, and their trajectories are fully determined by the interaction with the turbulent wave field and background plasma. A previous investigation of fast ion classical diffusion[22] shows that, in LAPD, pitch angle scattering is the dominant effect causing classical diffusion of the fast ions. Other effects such as Coulomb slowing down, and collision between fast ions and neutrals, typically have a time scale two orders of magnitude larger than Coulomb collision, thus they can be neglected for the current configuration.

Classical diffusion by pitch angle scattering is modeled by a Monte-Carlo collision operator.[35,36] The drift wave turbulence induced transport is modeled by following the trajectory of a fast ion within the background electric field fluctuation. For comparison with the experimental data, the calculated fast ion beam spatial profiles are recorded at the same positions as each observation port. Since the experimental signals average over many realizations of the drift-wave turbulence, a randomly selected sample of the com-

puted drift wave potential is chosen as the background turbulence at the beginning of each fast ion trajectory. When tracing each fast ion, the background field is assumed static and axially symmetric during the whole particle trajectory.
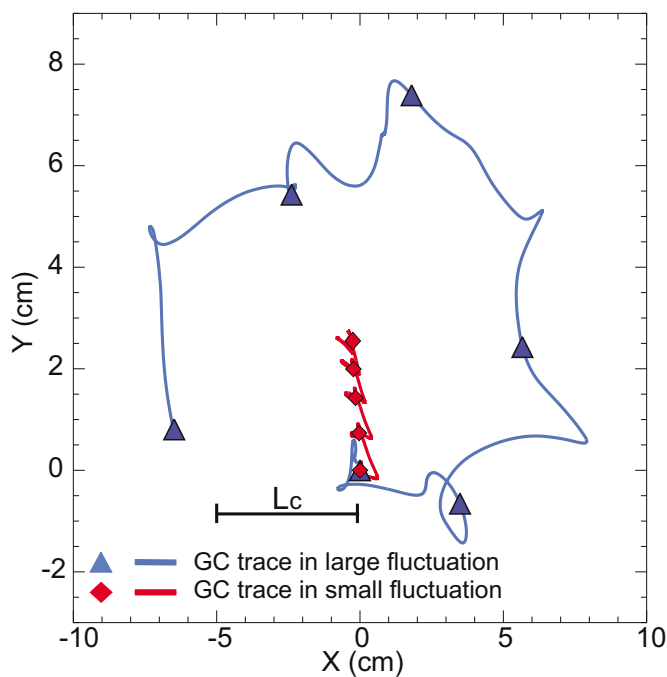
Without the turbulence, the fast ion transport, which is shown as the out of wave case in Fig. 14, is well described by classical diffusion theory. The simulated beam FWHM (Ref. 2) at 0–5 ports away from the initial position are consistent with the experimental data shown in Fig. 10, and the transport is diffusive.

The turbulent wave effect is then added into simulation. The reduction of classical transport due to the density depression by obstacle was not considered in the simulation, thus the classical transport effect is assumed the same for both cases. In Fig. 14, the in wave FWHM data show a good fit with Eq. (6) when Δr_0 and $D_\perp$ are set the same as the out of wave case. Like the experimental data, the simulation shows the ballistic nature of the fast ion transport for these conditions.

To confirm the physical mechanism of the transport, the relation between decorrelation and diffusive transport is demonstrated by following the gyrocenter (GC) trace of a single particle in turbulent wave fields of different amplitudes. Figure 15 displays the motion of the fast ion GC for two different wave amplitudes. When orbiting in a relatively small amplitude fluctuation, the drift of the fast ion GC drift (diamond) in each cyclotron period is small compared to the correlation length of the potential structure, which means that the fast ion is not decorrelated from the wave during its five cycles. Consequently, the GC shifts add approximately linearly over the entire trajectory, which yields a nondiffu-

sive transport. In contrast, for a stronger wave amplitude, the fast ion (triangle) drifts out of the correlation region. It is then able to sample a randomized potential field, and the transport is diffusive.

VI. CONCLUSIONS AND FUTURE WORK

In this experimental work, the energetic ion transport due to the turbulent drift wave is directly measured from the nonclassical spreading of the beam induced by the electrostatic potential field of the turbulence. The transport is observed to decrease as the fast ion energy increases. The time dependence of the transport is nondiffusive (ballistic), with the diffusive coefficient proportional to time. The mechanism of such transport is modeled and discussed. The energy dependence of the beam spreading is due to the gyroaveraging effect of fast ions with different orbit size. The nondiffusive nature of the transport is the result of the correlation between the fast ion trajectory and the turbulent potential structure. Both analytical model and simulation results provide good agreement with the experimental data.

Several extensions of this experimental study are possible. The transport of fast ions in electromagnetic waves is predicted[10] to differ from that in electrostatic waves. Fast ion transport in waves with a significant electromagnetic component can be obtained in LAPD by launching drift-Alfvén waves. Direct energy change of the fast ions by waves can be measured with a recently developed retarding field energy analyzer. Simulation result shows that the transport is diffusive when fast ions are decorrelated with the turbulent potential, which is also of great interest to observe experimentally.

ACKNOWLEDGMENTS

[1] A. Fasoli, C. Gormenzano, H. L. Berk, B. Breizman, S. Briguglio, D. S. Darrow, N. Gorelenkov, W. W. Heidbrink, A. Jaun, S. V. Konovalov, R. Nazikian, J.-M. Noterdaeme, S. Sharapov, K. Shinohara, D. Testa, K. Tobita, Y. Todo, G. Vlad, and F. Zonca, Nucl. Fusion **47**, S264 (2007).

[2] T. Hauff, F. Jenko, A. Shalchi, and R. Schlickeiser, Astrophys. J. **711**, 997 (2010).

[3] W. W. Heidbrink and G. Sadler, Nucl. Fusion **34**, 535 (1994).

[4] S. Günter, G. Conway, S. daGraça, H.-U. Fahrbach, C. F. M. G. Muñoz, and T. Hauff, Nucl. Fusion **47**, 920 (2007).

[5] T. Suzuki, S. Ide, T. Oikawa, T. Fujita, M. Ishikawa, and JT-60 Team, Nucl. Fusion **48**, 045002 (2008).

[6] H. Naitou, T. Kamimura, and J. M. Dawson, J. Phys. Soc. Jpn. **46**, 258 (1979).

[7] G. Manfredi and R. O. Dendy, Phys. Rev. Lett. **76**, 4360 (1996).

[8] G. Manfredi and R. O. Dendy, Phys. Plasmas **4**, 628 (1997).

[9] M. Vlad, F. Spineanu, S.-I. Itoh, M. Yagi, and K. Itoh, Plasma Phys. Controlled Fusion **47**, 1015 (2005).

[10] T. Hauff and F. Jenko, Phys. Plasmas **15**, 112307 (2008).

[11] T. Hauff, M. J. Pueschel, T. Dannert, and F. Jenko, Phys. Rev. Lett. **102**, 075004 (2009).

[12] W. Zhang, Z. Lin, and L. Chen, Phys. Rev. Lett. **101**, 095001 (2008).

[13] T. Hauff and F. Jenko, Phys. Plasmas **13**, 102309 (2006).

[14] H. Vernickel, M. Blaumoser, K. Ennen, J. Gruber, O. Gruber, O. Jandl, M. Kaufmann, H. Kollotzek, W. Köppendörfer, H. Kotzlowski, E. Lackner, K. Lackner, J. Neuhauser, J.-M. Noterdaeme, M. Pillsticker, R. Pöhlchen, H. Preis, K.-G. Rauh, H. Röhr, H. Schneider, W. Schneider, U. Seidel, B. Sombach, B. Streibl, G. Venus, F. Wesner, and A. Wieczoreka, J. Nucl. Mater. **128–129**, 71 (1984).

[15] J. L. Luxon, R. Anderson, F. Batty, C. B. Baxi, G. Bramson *et al.*, *Plasma Physics and Controlled Nuclear Fusion Research 1986* (IAEA, Vienna, 1987), Vol. I, p. 159.

[16] J. M. Park, M. Murakami, C. C. Petty, and W. W. Heidbrink, Phys. Plasmas **16**, 092508 (2009).

[17] W. W. Heidbrink, M. Murakami, J. M. Park, C. C. Petty, and M. A. V. Zeeland, Plasma Phys. Controlled Fusion **51**, 125001 (2009).

[18] G. Plyushchev, A. Diallo, A. Fasoli, I. Furno, B. Labit, S. H. Müller, M. Podestà, F. M. Poli, H. Boehmer, W. W. Heidbrink, and Y. Zhang, Rev. Sci. Instrum. **77**, 10F503 (2006).

[19] G. Plyushchev, "Interaction of suprathermal ions with turbulence in magnetized toroidal plasma," Ph. D. thesis, Ecole Polytechnique Fédérale de Lausanne, 2009.

[20] W. Gekelman, H. Pfister, Z. Lucky, J. Bamber, D. Leneman, and J. Maggs, Rev. Sci. Instrum. **62**, 2875 (1991).

[21] T. A. Carter, Phys. Plasmas **13**, 010701 (2006).

[22] L. Zhao, W. W. Heidbrink, H. Boehmer, and R. McWilliams, Phys. Plasmas **12**, 052108 (2005).

[23] Y. Zhang, W. W. Heidbrink, H. Boehmer, R. McWilliams, and S. Vincena, Phys. Plasmas **15**, 102112 (2008).

[24] Y. Zhang, W. W. Heidbrink, S. Zhou, H. Boehmer, and R. McWilliams, Phys. Plasmas **16**, 055706 (2009).

[25] M. V. Umansky, X. Q. Xu, B. Dudson, L. L. LoDestro, and J. R. Myra, Comm. Comp. Phys. **180**, 887 (2009).

[26] S. L. Chen and T. Sekiguchi, J. Appl. Phys. **36**, 2363 (1965).

[27] H. Boehmer, D. Edrich, W. W. Heidbrink, R. McWilliams, and L. Zhao, Rev. Sci. Instrum. **75**, 1013 (2004).

[28] Y. Zhang, H. Boehmer, W. W. Heidbrink, and R. McWilliams, Rev. Sci. Instrum. **78**, 013302 (2007).

[29] T. A. Carter and J. E. Maggs, Phys. Plasmas **16**, 012304 (2009).

[30] E. T. Everson, P. Pribyl, C. G. Constantin, A. Zylstra, D. Schaeffer, N. L. Kugland, and C. Niemann, Rev. Sci. Instrum. **80**, 113505 (2009).

[31] F. F. Chen, *Plasma Physics and Controlled Fusion* (Plenum, New York, 1984), p. 219.

[32] R. McWilliams and M. Okubo, Phys. Fluids **30**, 2849 (1987).

[33] G. I. Taylor, Proc. London Math. Soc. **s2-20**, 196 (1922).

[34] P. Popovich, M. V. Umansky, T. A. Carter, and B. Friedman, "Modeling of plasma turbulence and transport in the Large Plasma Device," Phys. Plasmas (unpublished).

[35] A. H. Boozer and G. Kuo-Petravic, Phys. Fluids **24**, 851 (1981).

[36] A. H. Boozer, Phys. Plasmas **9**, 4389 (2002).